Experimental Investigation of Fluid-Structure Interaction in Mach 2 Flow Using Simultaneous High-Speed PIV and DIC

Yoo-Jin Ahn*, Marc A. Eitner, Sina Rafati, Mustafa N. Musta, Jayant Sirohi, Noel T. Clemens

Dept. of Aerospace Engineering and Engineering Mechanics, The University of Texas at Austin, United States
*Corresponding author: yoojinahn@utexas.edu

Keywords: High-Speed PIV, Supersonic, Aerodynamics, FSI, DIC.

ABSTRACT

The fluid-structure interaction (FSI) of a compliant panel under a compression-ramp-induced shock/boundary-layer interaction (SBLI) has been studied in Mach 2 flow. Simultaneous high-speed measurements of the velocity field and the panel displacement were conducted using $50\,kHz$ particle image velocimetry (PIV) and $5\,kHz$ stereoscopic digital image correlation (DIC). The mean effect of the panel displacement has been evaluated by monitoring the change in velocity profiles along the streamwise direction (x), upstream of the separated flow region. Streamwise (u) velocity near the panel surface has been shown to change its magnitude in response to the wall shape. Furthermore, the strong cross-correlation between fluctuations of the wall-normal panel displacement and the transverse (v) velocity can be explained by the flow remaining tangent to the wall surface as the panel deforms. This latter result is consistent with the panel motion being sufficiently low frequency compared to flow convective time scales that the flow is quasi-steady. In addition, assessment of the correlation between the separation shock position and panel displacement seems to suggest that when the panel is bulged down (concave up) at the downstream end of the panel, a larger separated flow is generated and the shock moves upstream. This observation remains speculative, but is consistent with the flow undergoing greater compression for the bulged down case.

1. Introduction

Fluid-structure interaction (FSI) is a phenomenon where the vibrational response of the structure couples to the flow dynamics. With an increasing interest in the development of the next generation supersonic/hypersonic vehicles, rockets, and missiles, understanding this aerothermoelastic problem has become more relevant (McNamara & Friedmann, 2011). For instance, in high-speed flight, the frictional heating of the flow can weaken the panel and lead to increased compliance in the structure. Such compliance can be particularly important when the structure interacts with the intense pressure loading resulting from shock/boundary-layer interactions (SBLI) as they exhibit low-frequency unsteadiness that can readily couple to the structural dynamics (Dolling, 2001).

A number of experimental efforts have been made to study FSI with compliant panels underneath SBLIs. For example, Spottwood et al. (S. Spottswood et al., 2012; S. M. Spottswood et al., 2013, 2019) studied the response of compliant panels that were excited by a reflected shock interaction, and measured the coupling between the pressure field and the panel vibration. They found that the structural displacement induced pressure fluctuations at the dominant first mode frequency of the panel. Varigonda et al. (Varigonda & Narayanaswamy, 2019) have observed similar results in their FSI study. They observed shock oscillations to occur at the fundamental modes of the panel and a larger shock-foot intermittent region was observed for the compliant panel as compared to the rigid panel. Schöneich and Whalen (Schöneich et al., 2021) studied the fluid-thermal-structural interaction in a Mach 6 tunnel. They showed that there was a modal frequency shift of the panel due to different flow conditions induced by varying ramp angles and Reynolds numbers. Many other groups (Neet & Austin, 2020; Tripathi et al., 2021; Vasconcelos et al., 2021; Willems et al., 2013) have been active in the field to study the dynamics of FSI utilizing various displacement, pressure, and velocity measurement techniques.

Numerical simulations have also been used to investigate the coupling between the flow field and the structure. Visbal (Visbal, 2012) studied the interaction of an impinging shock on an infinite-length panel at supersonic speed. The simulated coupling showed that the panel flutter was influenced by the strength of the shock. With the presence of a shock, the panel showed a larger amplitude and frequency. Ostoich (Ostoich et al., 2013) used direct numerical simulation to study FSI of a thin panel in a Mach 2.25 turbulent boundary layer. The simulated thin panel motion induced the oscillating compression waves in time. When they compared the flow solutions from rigid and compliant panel cases, the differences were subtle. Still, Reynolds shear stress was found to be altered with panel vibratory motions.

This current paper is a continuation of the ongoing FSI research being conducted at UT Austin including, but not limited to, Goller (2019); M. A. Eitner et al. (2021); Musta et al. (2021); Ahn et al. (2022). These previous papers have explored the relationship between the unsteady surface pressure field and the panel deformation of the compliant panel under a ramp-induced SBLI. The compression ramp is placed at the downstream edge of the panel and so it is forced only at the downstream 25% of the panel length. Simultaneous pressure sensitive paint (PSP) —digital image correlation (DIC) measurements have shown that the first fundamental panel modes affect the shock-foot oscillation while the second mode seems to be influenced by the shock motion. In this study, the flow field measurement using a high-speed particle image velocimetry (PIV) synchronized with high-speed DIC has been conducted to investigate the interactions between the flow and the panel displacement.

2. Experimental Set-up

2.1. Facility and Wind Tunnel Model

The experiments were conducted in a Mach 2 wind tunnel located at The University of Texas at Austin. The wind tunnel used is a blow-down facility that can also be operated at $M_\infty = 5$ using a different nozzle block. For this specific test campaign, all tests were performed at Mach 2. The flow was not heated and it resulted in stagnation conditions of $T_0 = 285 \pm 3\,K$ and $p_0 = 345 \pm 5\,kPa$. The test section freestream velocity was measured to be approximately $U_\infty = 513\,m/s$ and the boundary-layer thickness was estimated to be $\delta_{99} = 10.3\,mm$. The freestream turbulence intensity was about 1.2% and the freestream Reynolds number was around $Re_\infty = 3.9 \times 10^7\,m^{-1}$.

The shock-wave boundary interaction was generated by a 20°compression ramp, which is $101.5\,mm$ in width. It was installed spanwise-centered inside the $152\,mm$ wide test section. Since there is a space of $25\,mm$ between the tunnel wall and the edge of the compression ramp, it was fitted with fences that extend about $10\,mm$ upstream to prevent interactions with the corner vortices. The panel was mounted into a floor plug so that it is flush with the test section floor. As shown in figure 1, the ramp is placed at the downstream edge of the panel.

A $1\,mm$ compliant panel was mainly used for the current test campaign. A non-compliant aluminum panel was also tested to provide a baseline case. Both panels have a dimension of $127\,mm \times 68.5\,mm$. The compliant panel was manufactured from a single block of polycarbonate and included a thicker flange to provide rigid support around the edges ($1.27\,mm$ in thickness) of the panel. The first three modal frequencies were calculated in M. Eitner et al. (2021) and measured through impact tests (tab. 1). It should be noted that the modal frequencies can vary up to $\pm 100\,Hz$ depending on the pressure differential across the panel. A pressure-controlled cavity, mounted underneath the panel, was used to maintain a low differential pressure across the panel. The cavity was operated at sub-atmospheric pressures because the test section pressure is nominally 0.4 atm absolute. The cavity pressure was set using a vacuum pump and pressure transducer. The pressure was usually set to match the free-stream pressure inside the test section, but since the SBLI leads to a non-uniform pressure distribution over the surface, there is no single pressure value that ensures zero mean deflection. The cavity also has a window to allow an unobstructed view of the back surface for displacement measurement using DIC.

Table 1. Calculated and measured natural frequencies of the panel in quiescent air

	Mode 1, Hz	Mode 2, Hz	Mode 3, Hz
Calculated	349	473	675
Measured	407	542	N/A

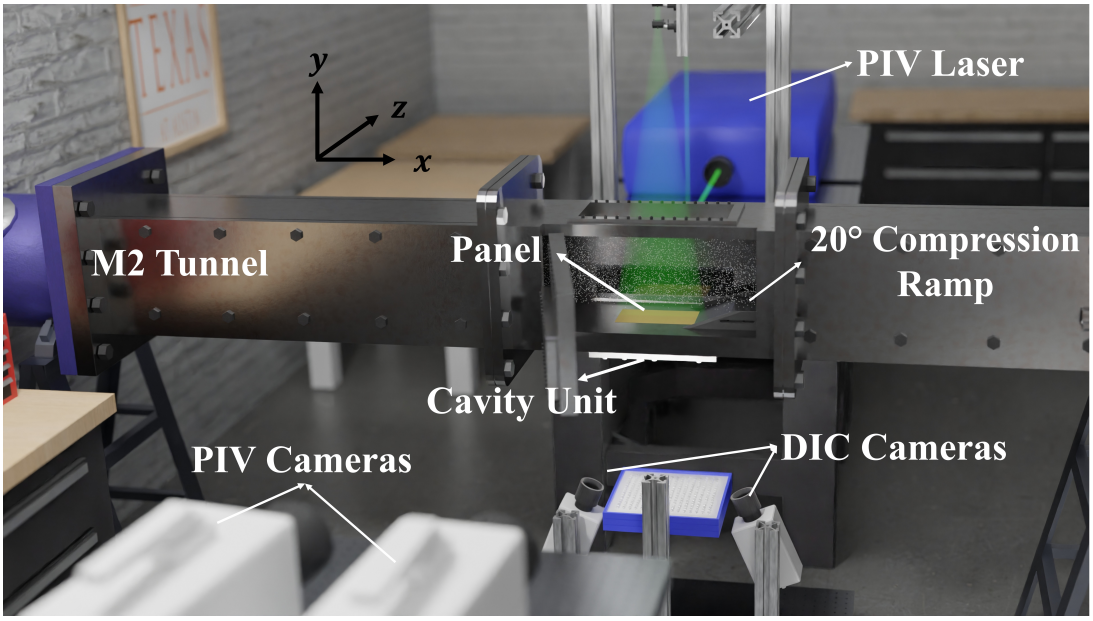

Figure 1. Graphic of the experimental set up and the coordinate system

2.2. High-Speed Particle Image Velocimetry (PIV)

High-speed ($50\,kHz$) planar PIV was conducted in the streamwise (x) - wall-normal (y) plane. The plane was selected on the spanwise-center location of the panel (fig. 3). An Nd:YAG frequency-doubled pulse-burst laser (Spectral Energies 'QuasiModo') was used as the light source. The laser produces $10.5\,ms$ bursts of evenly spaced pulse-doublets ($1500\,ns$ apart) at $50\,kHz$ with a center wavelength of $532nm$. Using a series of optics, an approximately $1mm$ thick laser sheet was created and it was introduced to the test section from the top of the tunnel. (fig. 1)

Two Photron Fastcam SA-Z cameras, equipped with Scheimpflug adaptors and $200\,mm$ Nikon lenses, were used to image the particle fields. Both cameras were slightly angled to make sure that they have an overlapping field of view of at least 10% for the "stitching process" (fig. 2). The stitched field of view is described in figure 2. It extends up to 3/4 of the panel length from the ramp corner and to about $1.5\delta_{99}$ on the compression ramp surface. The cameras were operated at $100\,kHz$ with a resolution of 640×280 pixels for each camera. LaVision DaVis v10.1 was used to stitch the image field together and process the particle images. A multiplass, elliptical interrogation scheme was used with a final window size of 32×32 pixels (75% overlap). The resulting spatial resolution was approximately $0.0872\,mm$ per pixel and $2.79\,mm$ per window.

For seeding particles, titanium dioxide (TiO_2) particles with a primary particle size of $20\,nm$ were used. The particles were baked in an oven for at least 12 hours prior to the testing to lower the moisture content and thus reduce the tendency of the particles to agglomerate. The particles were seeded into the plenum using a fluidized bed followed by a cyclone separator to extract the smallest particles.

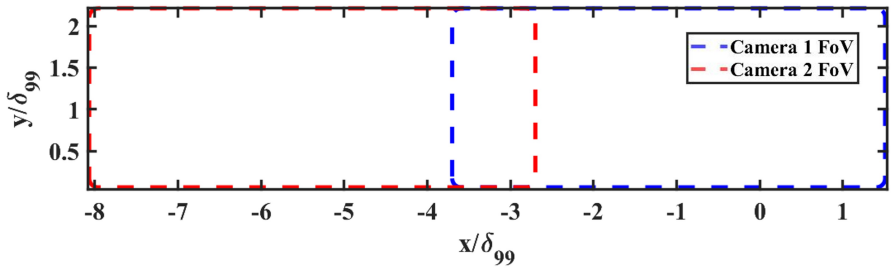

Figure 2. Fields of view of two PIV cameras and the coordinate system in x-y plane. (The ramp starts from $x/\delta_{99} = 0$.)

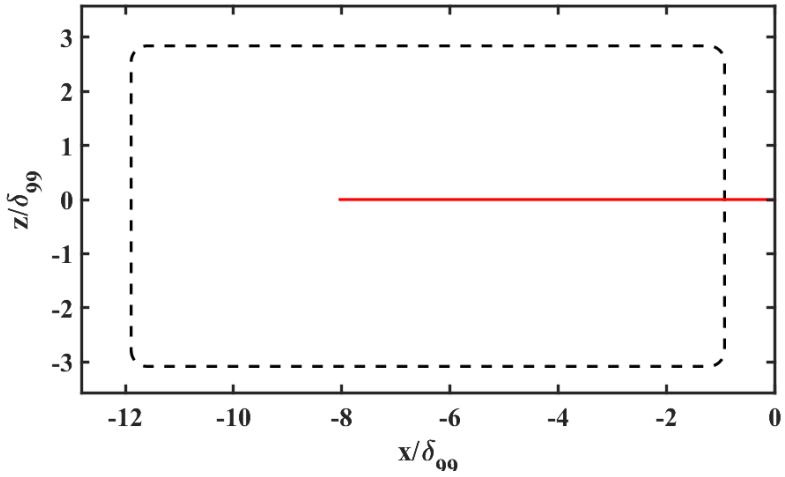

Figure 3. Top view of the entire panel and the coordinate system in x-z plane. Black dash line indicates the DIC field of view. Red line is the line along the PIV plane. (The ramp starts from $x/\delta_{99} = 0$.)

2.3. Stereoscopic Digital Image Correlation (DIC)

The out-of-plane (y-direction) panel displacement (h) was measured using stereoscopic DIC. The random speckle pattern, required for the DIC technique, was generated by printing the pattern onto a paper sticker and affixing it to the back of the compliant panel.

Two high-speed cameras (Vision Research Miro M310) fitted with Scheimpflug adapters and $105\,mm$ Nikon lenses were placed underneath the tunnel to view the backside of the panel (fig. 1). The DIC field of view is marked with a black dashed rectangle in figure 3. Recorded images were processed through LaVision DaVis v10.1 to calculate the correlations, by setting an interrogation window size of 31×31 pixels with 7 pixel overlap. Displacement data around the edge of the panel back surface (approximately $8\,mm$ from the edge) could not be captured due to the spatial resolution of the current DIC system.

3. Results

3.1. Streamwise and Wall-Normal Velocity Fields

For each set of experiments, data were collected for $10.5\,ms$. The limitation in the duration of data collection was due to the nature of the pulse burst laser. $10.5\,ms$ of $50\,kHz$ PIV resulted in 510 frames of the velocity field. However, due to the motion of the surface, at some times surface reflections precluded acceptable vector fields to be computed. For this reason, the time records used were typically shorter than $10.5\,ms$. Four PIV sets with 400 to 500 frames for each set were acquired in total.

The planar PIV yielded two velocity components: u (streamwise velocity) and v (wall-normal velocity). Sample time sequences of both components normalized to the freestream velocity are presented in figure 4. The time-resolved u-velocity field provided in figure 4a effectively captures turbulent structures convecting downstream, as well as the separation bubble breathing near the ramp corner (Babinsky & Harvey, 2011). The v contour shows an abrupt change in velocity near the ramp side: from around $0.01U_\infty$ to $0.1U_\infty$ (fig. 4b). Although the exact location of the separation shock cannot be tracked due to the poor spatial resolution of the high-speed PIV, the abrupt change in v-velocity roughly indicates the location of the separation shock.

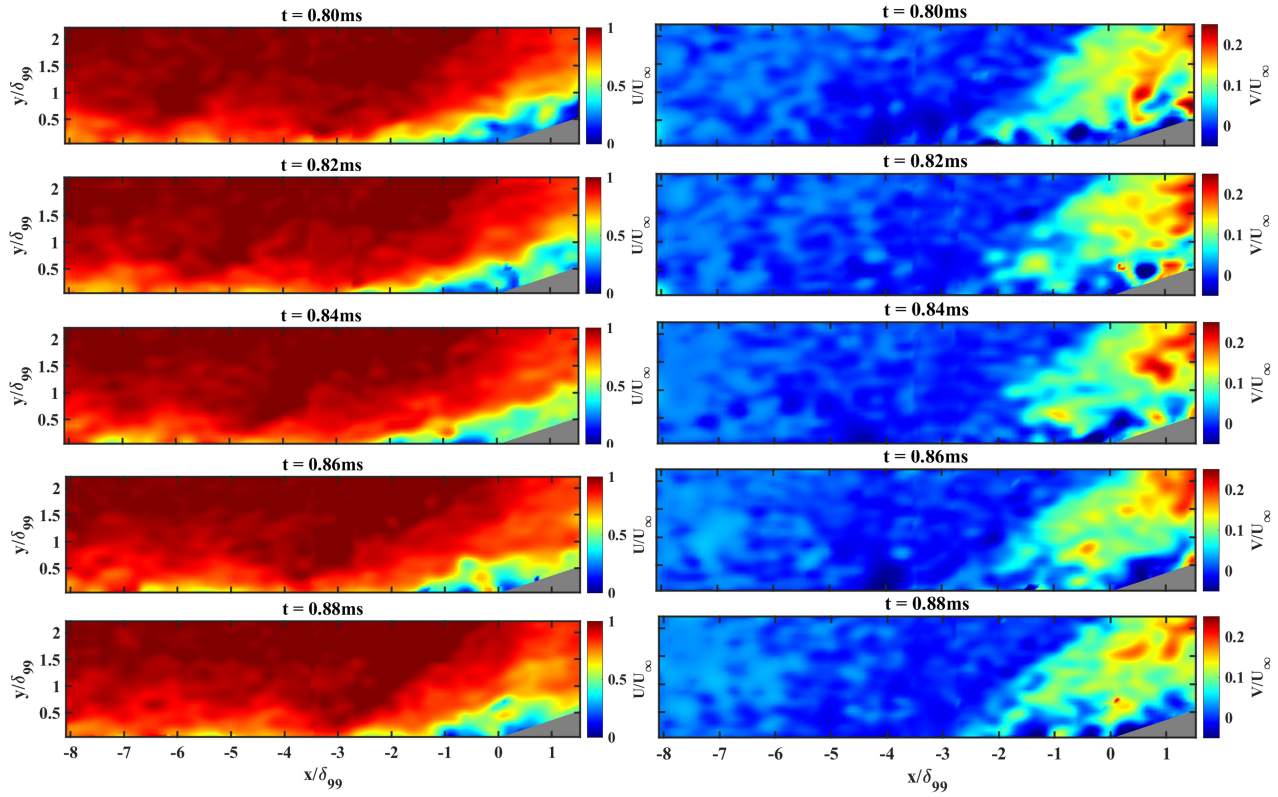

(a) Normalized streamwise u-velocity

(b) Normalized wall-normal v-velocity

Figure 4. Sample time sequence of velocity fields normalized to the freestream velocity (test #4)

3.2. Out-of-Plane Displacement Field

The stereo-DIC system measured the out-of-plane displacement (h) field (y-direction). The mean displacement over the entire time period of the DIC measurement is plotted in figure 5 —positive values indicate the panel bulging inward to the tunnel and the opposite is true for negative values. For better visualization, the mean deformation along the spanwise-centerline of the panel is shown along with the maximum and minimum excursions from the mean (dashed lines) (fig. 6).

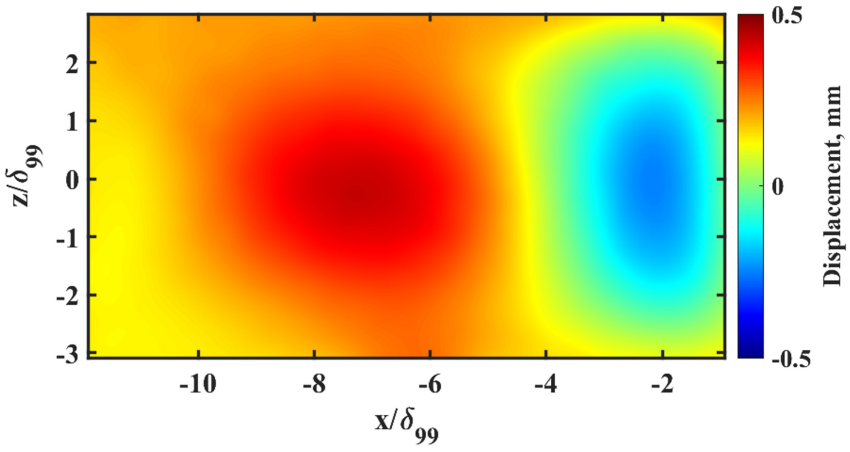

Figure 5. Mean displacements field in x-z plane (test #3)

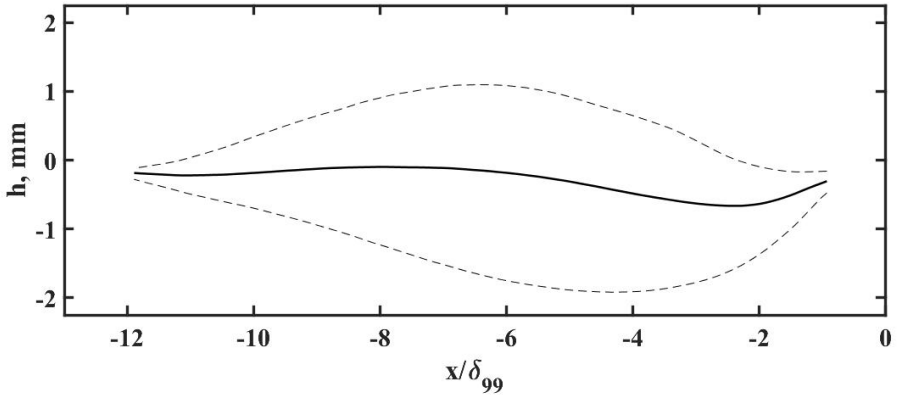

Figure 6. Mean panel displacement along the spanwise centerline (black solid line) and the maximum and minimum excursion of the panel displacement (black dash line) (test #3)

The external-pressure of the panel was manually, but carefully, controlled using a vacuum pump to match the static pressure of the flow (around $0.4\,atm$) (M. A. Eitner, 2021). However, due to leaks in the system, the cavity pressure tended to vary somewhat from run to run. The variation in the cavity pressure resulted in variation in the mean panel displacement from run to run. Figure 7 points out that with higher back-pressure, the panel is mostly pushed into the test section. The trend in shape seems to be consistent, however: the panel bulged inward in the upstream region

and a lower bump downstream due to the high pressure region after the shock. As mentioned in section 2.1, a shift in fundamental frequency due to the change in effective stiffness was also noticed. The spectral content of the vibratory motion near the center of the panel was evaluated for each test case. The dashed and dotted lines marked in figure 8 are the first and second modal frequencies from the impact tests, respectively (tab. 1).

The DIC cameras were recorded for 2 seconds, which is much longer than the data collection time of the PIV system. A portion of the mean-subtracted centerline displacement (h') field is plotted in figure 9. The x-axis indicates the normalized streamwise coordinate; the y-axis is time. The overlapping field of view and measurement time of PIV is marked with a black dashed rectangle.

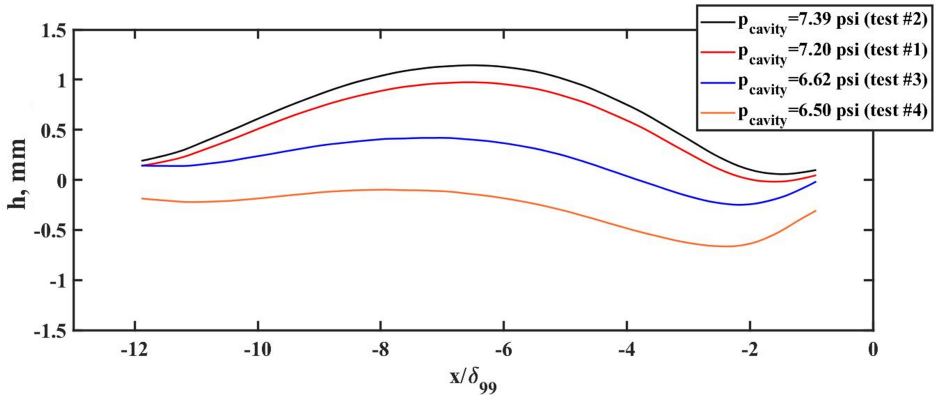

Figure 7. Spanwise-centerline profiles of different mean displacement with varying cavity pressure over the time interval of the PIV measurement

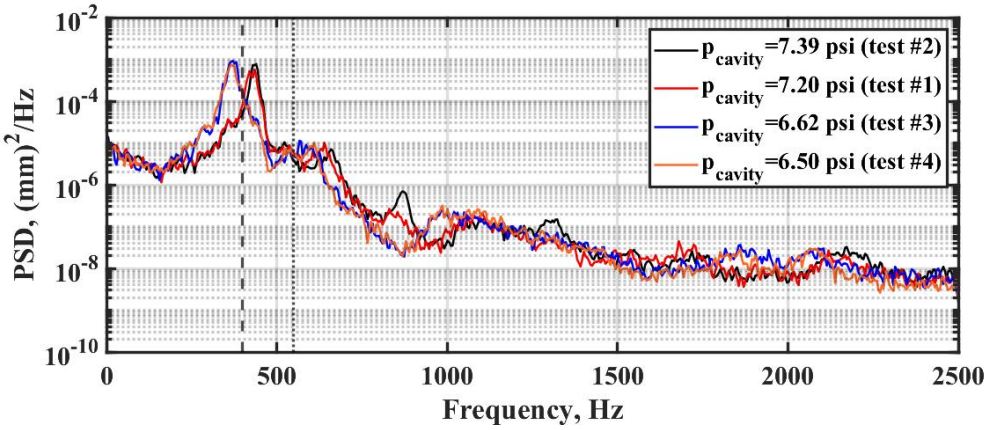

Figure 8. Spectral contents of displacement at the location near the center of the panel with the vibratory modes from impact tests marked in dashed (mode 1) and dotted (mode 2) lines

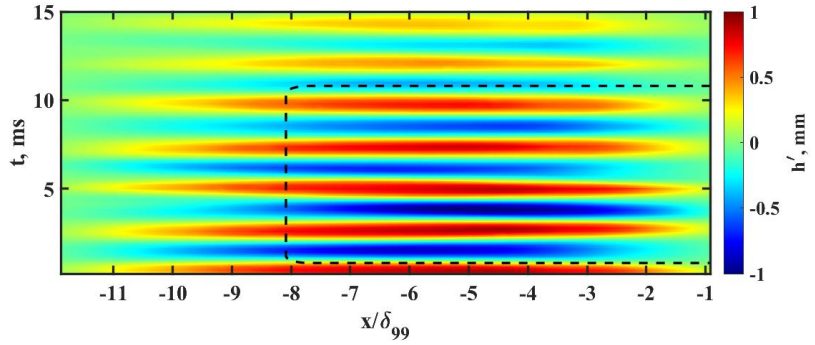

(a) test #1

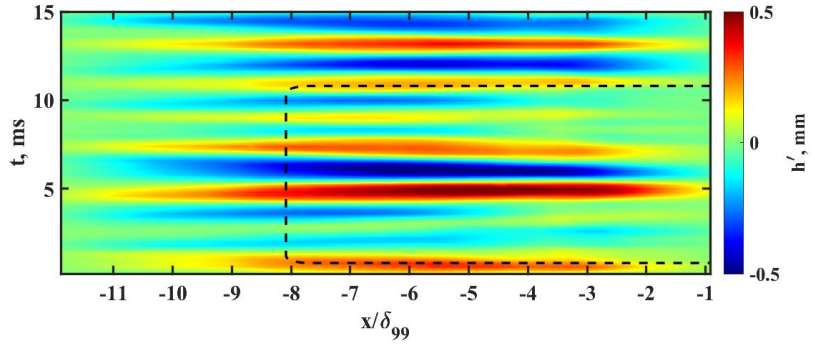

(b) test #2

Figure 9. Centerline mean-subtracted panel displacements in time from t = 0 to 15 ms (x-t)

3.3. Mean Effect of the Structure Deformation on the Velocity

The mean displacement profiles (fig. 7) suggest that the flow near the wall would go through gradual changes in its velocity. One can speculate that as the wall deflection angle or the "slope" along the x-direction (dh/dx) becomes larger with positive values, the flow would be steadily compressed. The flow would expand in the opposite case.

Figure 10 (a) and (b) compare the mean velocity contours of rigid and complaint cases, respectively. There seems to be an overall shift in velocity field due to the displaced panel. The speculated velocity changes near the surface are not easily discernible "by eye". Instead, the mean velocity profiles at different streamwise locations have been evaluated. To take into account for the deformed surface, the y-coordinate of each plot has been modified to make sure that it correctly represents the distance from the wall. This corrected wall normal coordinate is defined as y^*.

Unlike the rigid panel case (fig. 11a), the compliant panel does not have consistent velocity profiles (fig. 11b). The velocities converge with distance from the wall, but near the surface, there is a velocity difference of $0.25U_\infty$ (y^*/δ_{99} = 0.097). The observed deceleration is in line with the previous assumption: compression along the positive wall deflection from x/δ_{99} = -8 to -7 (fig. 7). The same has been calculated along the negative slope from x/δ_{99} = -7 to -3 (fig. 7). u/U_∞ increases from 0.75 to 0.81 (y^*/δ_{99} = 0.097) resulting in a fuller velocity profile (fig. 11c). The mean effect of the panel

deformation is reflected in the flow field.

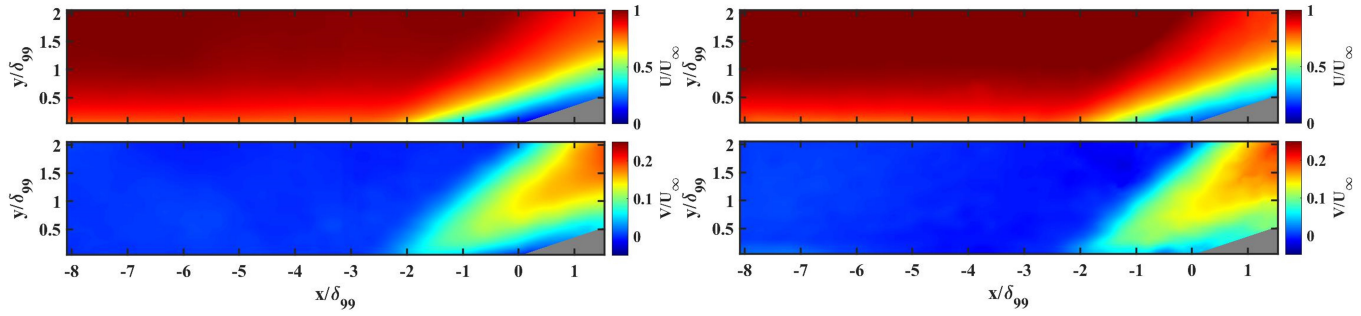

(a) Rigid panel: Normalized mean velocity fields

(b) Compliant panel (test #4): Normalized mean velocity fields

Figure 10. Comparison of the mean u- and v-velocity fields

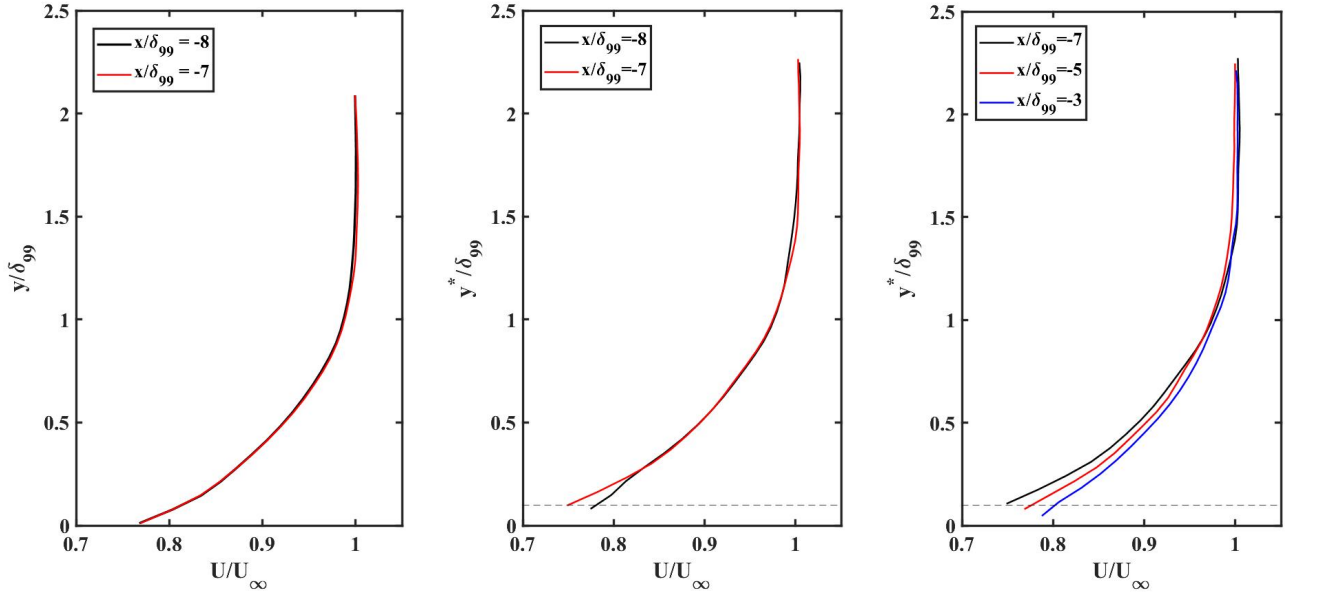

(a) Rigid panel: x/δ_{99} = -8, -7

(b) Compliant panel (test #4): x/δ_{99} = -8, -7

(c) Compliant panel (test #4): x/δ_{99} = -7, -5, -3

Figure 11. Comparison of velocity profiles at different streamwise locations for rigid and compliant cases.

3.4. Cross-Correlations Between Displacement and Velocity Fluctuations

The panel's dominant first-mode frequency is about $400\,Hz$ (tab. 1 and fig. 8), and so the time required for the panel to complete one cycle of this motion (τ_w = 0.0025 sec) is an order of magnitude longer than the time it takes for the flow to travel the panel length (τ_v = 0.00025 sec). Therefore, the flow can be considered quasi-steady as the panel undergoes its dominant vibratory motion especially in the upstream region.

The cross-correlation between the mean-subtracted out-of-plane displacement (h') and the fluctuation in wall-normal velocity (v') supports that assumption. The vector ordering of the cross-correlation was set so that v' vector gets shifted while computing the correlation but h' stays the

same. For the calculation, $5\,kHz$ DIC data was upsampled using spline interpolation to match the length of the velocity data. The v-velocity was taken at y/δ_{99} = 0.1, and then low-pass filtered at $2\,kHz$ to get rid of the high-frequency turbulent noise. Two different x locations on the panel shown in figure 12 were chosen for this investigation.

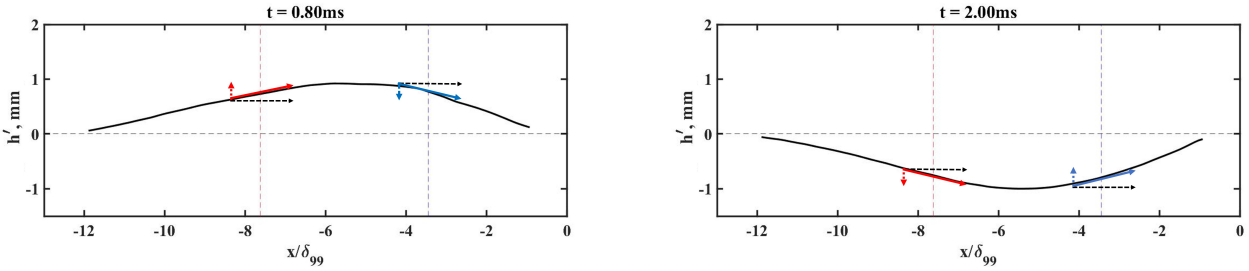

(a) Panel up

(b) Panel down

Figure 12. Plots of mean-subtracted panel displacement for cases where the panel is displaced up into the flow and down out of the flow. Also shown are arrows to represent the flow velocities that are tangent to the panel at two different streamwise locations (test #4)

At x/δ_{99} = -7.62 (a red dash line in fig. 12), the time series of two quantities demonstrate that the vertical velocity fluctuation seems to follow the movement of the panel (fig. 13a). This relationship is confirmed by the cross-correlation coefficient of 0.85, as shown in figure 13. On the other hand, at x/δ_{99} = -3.45 (a blue dash line in fig. 12), the waveforms seem to be anti-correlated and the peak negative cross-correlation coefficient (-0.64) confirms this (fig. 14). In this case, the v component of velocity is out of phase with the panel movement. It shows that the deformed panel surface affects the flow dynamics near the wall. The observed correlation between v' and panel displacement can be understood with the help of fig. 12. Consider the point at x/δ_{99} = -7.62, for the case where the panel is bulged up and down. Since the flow is quasi-steady, we expect the local flow velocity to be tangent to the wall. This flow direction is shown by the velocity vectors. When the flow is moving upward, then v' is positive, but when the flow is moving downward, then v' is negative. Therefore, we expect v' to have the same sign as the panel displacement, which is what is shown in fig. 13. However, if we consider the point at x/δ_{99} = -3.45 in fig. 12, we see that v' is negative when the panel displacement is positive, and *vice versa*. This leads to the two waveforms being anti-correlated, which is what we see in fig. 14.

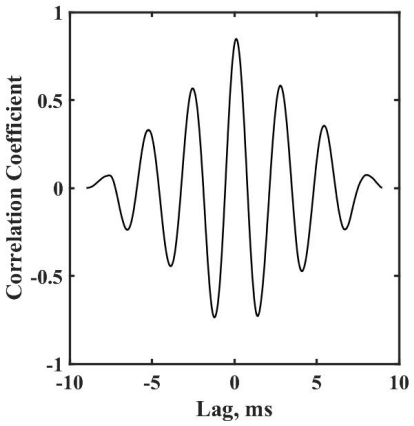

(a) Cross-correlation result

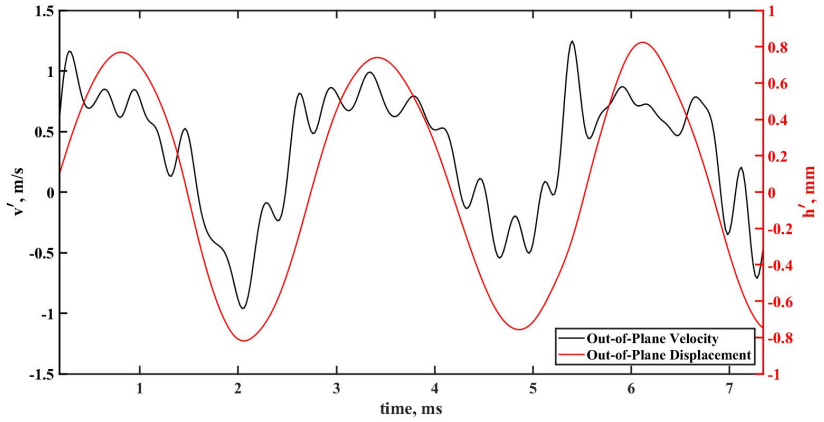

(b) Time series of v' and the mean-subtracted panel displacement

Figure 13. Time histories and cross-correlation between the mean-subtracted displacement and the wall-normal velocity fluctuation at x/δ_{99} = -7.62 (test #4)

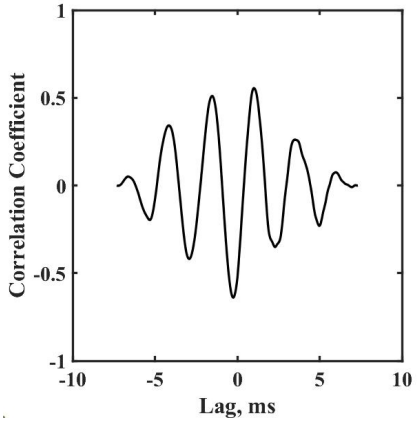

(a) Cross-correlation result

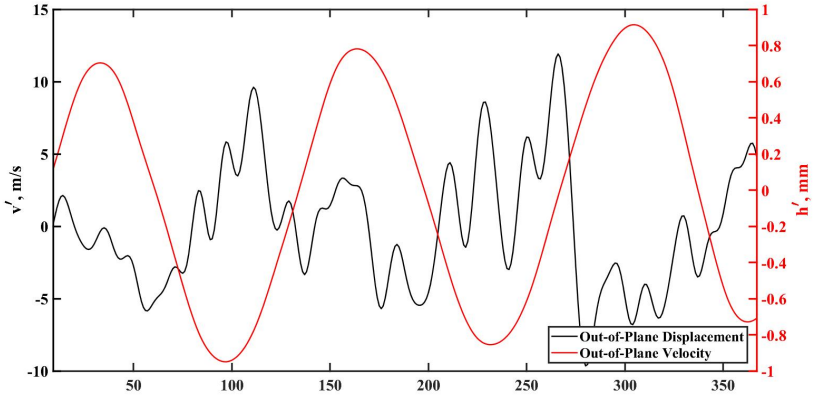

(b) Time series of v' and mean-subtracted panel displacement

Figure 14. Time histories and cross-correlation between the mean-subtracted displacement and the wall-normal velocity fluctuation at x/δ_{99} = -3.45 (test #4)

3.5. Surrogate Separation Shock Location

The surrogate separation shock location was tracked by detecting the line where the v-velocity component undergoes a sudden change in magnitude. A time sequence of v-velocity fields where the surrogate separation shock is identified using this method is shown in figure 15. A black dotted line shows the shock position that was found. The results are also plotted on the u-velocity field to make sure the located lines reasonably capture the physics of the separated region (fig. 16). The average x location of the surrogate line (y/δ_{99} from 0.7 to 1.1) was recorded for each frame. The detected locations seem to represent the change in the separated region fairly well.

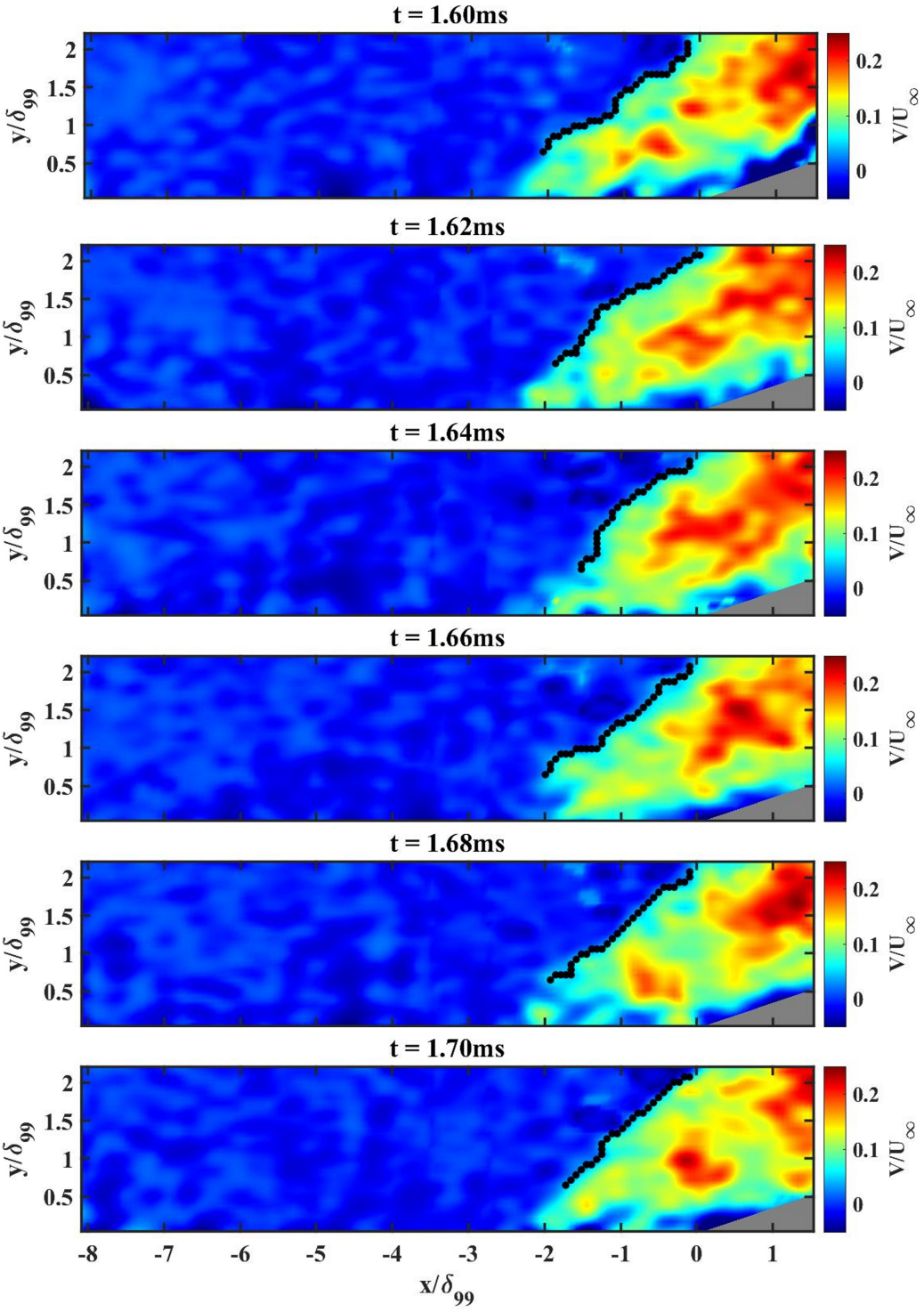

Figure 15. Time sequence of the v-velocity with the surrogate separation shock marked with dots (test #4)

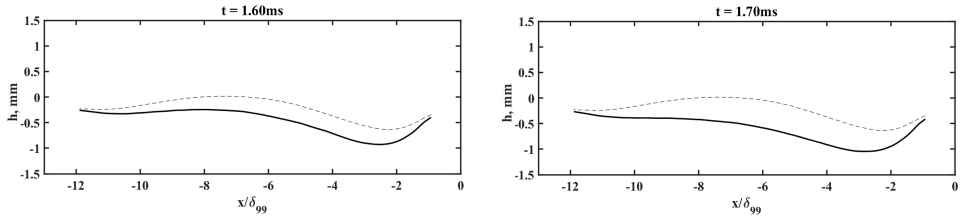

(a) Change in panel surface from $t = 1.6 \sim 1.7\,ms$

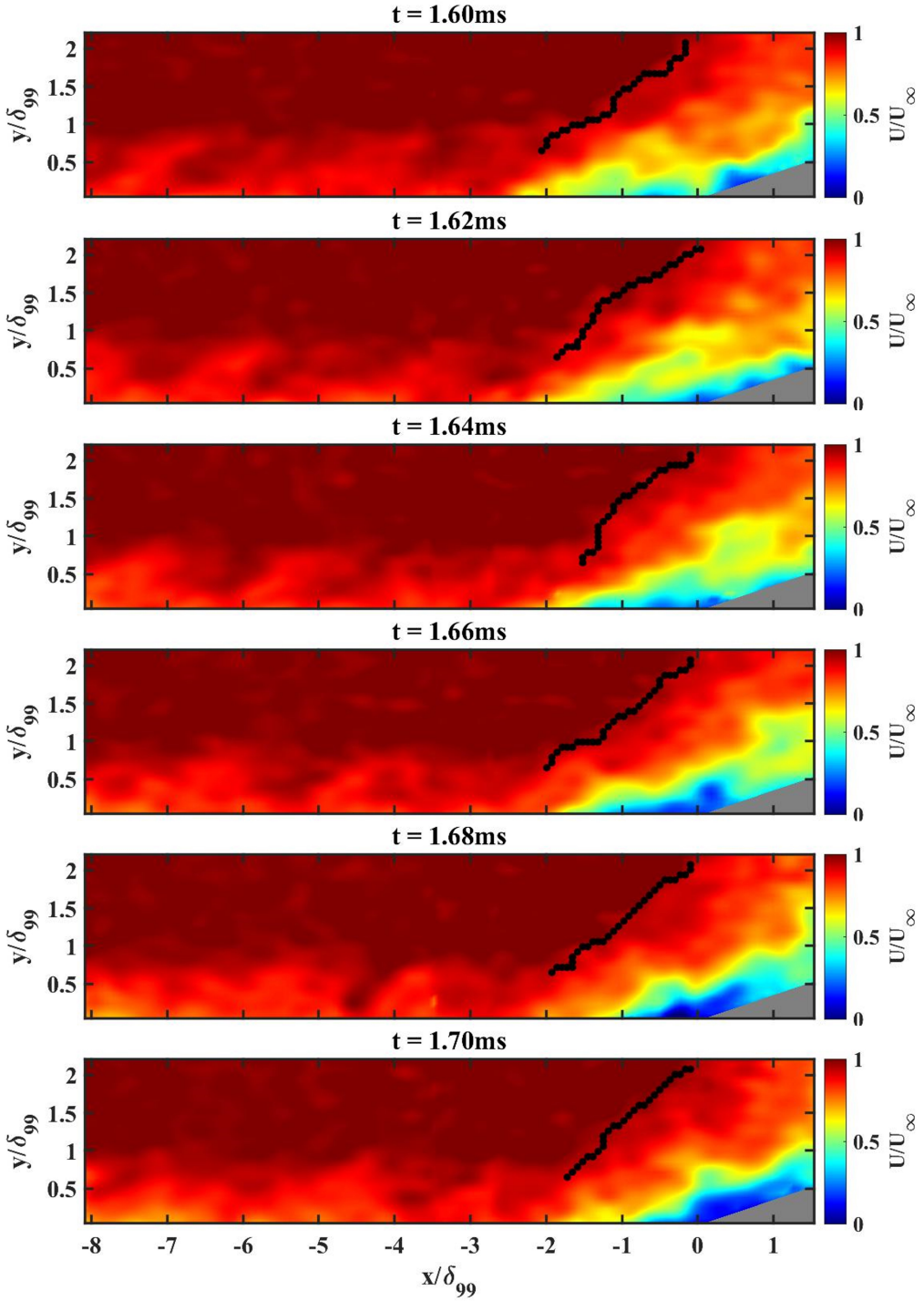

(b) Time sequence of the u-velocity with the surrogate separation shock marked with dots

Figure 16. Time sequence of displacement and velocity where the slope (dh/dx) near x/δ_{99} = -1.5 is positively increasing (test #4)

The panel displacement at x/δ_{99} = -1.5 (near the ramp) is plotted over the change of the surrogate separation location (fig. 17) for test cases #1 and #2. There does not seem to be a definitive relation between the two. One observation made: when the wall deflection is positive and is increasing, the size of the separation bubble tends to grow. The larger slope at the aft end of the panel means that the panel is bulging downward (i.e., concave upward), meaning the panel is forming a shallow cavity-like space near the compression corner. It seems plausible that this additional cavity causes the flow to undergo a stronger compression and hence causes a larger separation bubble to form. A sequence provided in figure 16 is also an example of the described panel motion from test #4. As expected, the separation bubble is growing. However, it should be noted that this is merely a speculation based on the observation made with limited number of data sets.

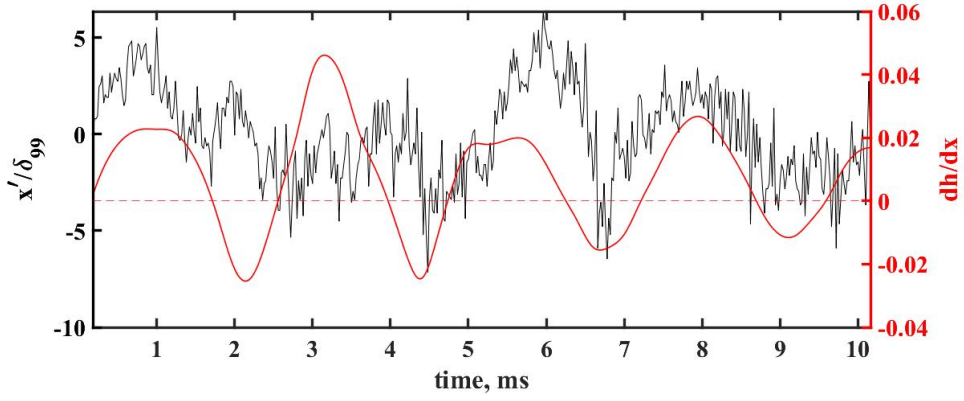

(a) test #1

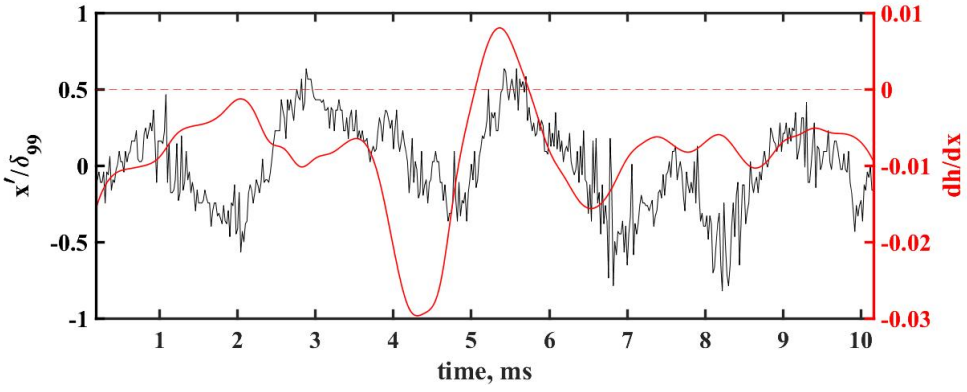

(b) test #2

Figure 17. Fluctuation of the surrogate shock location (black line) and the change in slope at x/δ_{99} = -1.5 (red line)

The formation of a positive wall deflection upstream of the compression ramp is subjected to various conditions, including the amplitude of the panel oscillation. The mean panel profiles of tests #1 and #2 have a nominally similar shape (fig. 7). However, test #2 has a much smaller amplitude displacement than that for test #1, at least for the limited time period when the velocity data was collected (fig. 9). Test #2 forms the concave-up surface only in the time period between $t = 5.06 \sim 5.72\,ms$ where strong enough panel vibration takes place. Previous studies in this facil-

ity used DIC and pressure sensitive paint to establish that the shock-foot motion is locked to the first fundamental mode of the panel and Eitner (M. A. Eitner, 2021) has also demonstrated that such frequency relation becomes stronger with higher displacement amplitude. The wall shape upstream of the compression ramp may be one possible explanation of such coupling. Again, more in-depth investigation with a larger data set is required at this point.

4. Conclusions

The current study investigated a thin panel response to a compression-ramp-induced SBLI in Mach 2 flow. The velocity and panel displacement were simultaneously measured using $50\,kHz$ planar PIV and $5\,kHz$ stereo-DIC, respectively. The results suggest that the mean shape of the panel affected the flow near the wall. The change in the upstream boundary layers suggests that the flow decelerates as it encounters a positive wall deflection angle, and accelerates when is encounters a negative wall deflection angle. A similar effect has been found in the velocity fluctuations. The cross-correlation functions between the out-of-plane displacement and the wall-normal velocity (v) support the fact that the flow travels along the deformed surface as the v-velocity increases or decreases with the wall displacement. These observations are all consistent with a flow that is quasi-steady in the presence of panel vibration. Although more detailed analysis is needed, the time series of the surrogate separation shock location and the wall deflection imply that the bulged out surface near the ramp may be affecting the dynamics of the shock system.

Acknowledgements

This work is supported by the National Science Foundation under award # 1913587. This support is gratefully acknowledged.

Nomenclature

x	Streamwise direction
y	Wall-normal direction
z	Cross-flow direction
u	Streamwise velocity component [m/s]
v	Wall-normal velocity component [m/s]
v'	Root-mean-square fluctuation of wall-normal velocity [m/s]
h	Out-of-plane panel displacement [mm]
h'	Mean-subtracted displacement [mm]
dh/dx	Wall deflection [AU]

References

Ahn, Y.-J., Musta, M. N., Eitner, M. A., Sirohi, J., & Clemens, N. T. (2022). Experimental investigation of flow-structure interaction for a compliant panel under a mach 2 compression-ramp. *AIAA Scitech Forum*, paper 2022-0293.

Babinsky, H., & Harvey, J. K. (2011). *Shock wave-boundary-layer interactions* (Vol. 32). Cambridge University Press.

Dolling, D. S. (2001). Fifty years of shock-wave/boundary-layer interaction research: what next? *AIAA Journal*, *39*(8), 1517–1531.

Eitner, M., Musta, M., Vanstone, L., Sirohi, J., & Clemens, N. (2021). Modal parameter estimation of a compliant panel using phase-based motion magnification and stereoscopic digital image correlation. *Experimental Techniques*, *45*(3), 287–296.

Eitner, M. A. (2021). *Experimental investigation of fluid-structure interaction of a compliant panel under a mach 2 compression ramp shock-boundary layer interaction* (PhD Dissertation). The University of Texas at Austin.

Eitner, M. A., Ahn, Y.-J., Vanstone, L., Musta, M. N., Sirohi, J., & Clemens, N. (2021). Effect of shock-wave boundary layer interaction on vibratory response of compliant panel. *AIAA Aviation Forum*, paper 2021-2493.

Goller, T. J. (2019). *Simultaneous high-speed displacement and surface pressure measurements of a compliant panel under a mach 2 compression ramp interaction* (Master's Thesis). The University of Texas at Austin.

McNamara, J. J., & Friedmann, P. P. (2011). Aeroelastic and aerothermoelastic analysis in hypersonic flow: past, present, and future. *AIAA journal*, *49*(6), 1089–1122.

Musta, M. N., Vanstone, L., Ahn, Y.-J., Eitner, M., Sirohi, J., & Clemens, N. (2021). Investigation of flow-structure coupling for a compliant panel under a shock/boundary-layer interaction using fast-response psp. *AIAA Aviation Forum*, paper 2021-2809.

Neet, M. C., & Austin, J. M. (2020). Effects of surface compliance on shock boundary layer interaction in the caltech mach 4 ludwieg tube. *AIAA Scitech Forum*, paper 2020-0816.

Ostoich, C. M., Bodony, D. J., & Geubelle, P. H. (2013). Interaction of a mach 2.25 turbulent boundary layer with a fluttering panel using direct numerical simulation. *Physics of Fluids*, *25*(11), 110806.

Schöneich, A. G., Whalen, T. J., Laurence, S. J., Sullivan, B. T., Bodony, D. J., Freydin, M., … Buck, G. M. (2021). Fluid-thermal-structural interactions in ramp-induced shock-wave boundary-layer interactions at mach 6. *AIAA Scitech Forum*, paper 2021-0912.

Spottswood, S., Eason, T., & Beberniss, T. (2012). Influence of shock-boundary layer interactions on the dynamic response of a flexible panel. *Proceedings of the ISMA-2012*, 17–19.

Spottswood, S. M., Beberniss, T. J., Eason, T. G., Perez, R. A., Donbar, J. M., Ehrhardt, D. A., & Riley, Z. B. (2019). Exploring the response of a thin, flexible panel to shock-turbulent boundary-layer interactions. *Journal of Sound and Vibration*, *443*, 74–89.

Spottswood, S. M., Eason, T., & Beberniss, T. (2013). Full-field, dynamic pressure and displacement measurements of a panel excited by shock boundary-layer interaction. In *19th aiaa/ceas aeroacoustics conference* (p. 2016).

Tripathi, A., Gustavsson, J., Shoele, K., & Kumar, R. (2021). Response of a compliant panel to shock boundary layer interaction at mach 2. *AIAA Scitech Forum*, paper 2021-0489.

Varigonda, S. V., & Narayanaswamy, V. (2019). Investigation of shock wave oscillations over a flexible panel in supersonic flows. *AIAA Aviation Forum*, paper 2019-3543.

Vasconcelos, P. B., McQuellin, L. P., Krishna, T., & Neely, A. (2021). Experimental study of hypersonic fluid-structure interactions on an inclined clamped-free-clamped-free compliant panel. In *Ascend 2021* (p. 4232).

Visbal, M. (2012). On the interaction of an oblique shock with a flexible panel. *Journal of Fluids and Structures*, *30*, 219–225.

Willems, S., Gülhan, A., & Esser, B. (2013). Shock induced fluid-structure interaction on a flexible wall in supersonic turbulent flow. *Progress in Flight Physics*, *5*, 285–308.